entropy

MDPI

Article

Analysis of Entropy Generation in Natural Convection of Nanofluid inside a Square Cavity Having Hot Solid Block: Tiwari and Das' Model

Mikhail A. Sheremet [1,2], Hakan F. Oztop [3,4], Ioan Pop [5,*] and Nidal Abu-Hamdeh [4]

Received: 9 November 2015; Accepted: 21 December 2015; Published: 31 December 2015
Academic Editors: Giulio Lorenzini and Omid Mahian

1 Department of Theoretical Mechanics, Faculty of Mechanics and Mathematics, Tomsk State University, 634050 Tomsk, Russia; Michael-sher@yandex.ru
2 Institute of Power Engineering, Tomsk Polytechnic University, 634050 Tomsk, Russia
3 Department of Mechanical Engineering, Technology Faculty, Fırat University, 23100 Elazig, Turkey; hfoztop1@gmail.com
4 Department of Mechanical Engineering, Engineering Faculty, King Abdulaziz University, 21589 Jeddah, Saudi Arabia; nabuhamdeh@kau.edu.sa
5 Department of Mathematics, Babeş-Bolyai University, 400084 Cluj-Napoca, Romania
* Correspondence: popm.ioan@yahoo.co.uk; Tel.: +40-264-405-300

Abstract: A computational work has been performed in this study to investigate the effects of solid isothermal partition insertion in a nanofluid filled cavity that is cooled via corner isothermal cooler. Mathematical model formulated in dimensionless primitive variables has been solved by finite volume method. The study is performed for different geometrical ratio of solid inserted block and corner isothermal cooler, Rayleigh number and solid volume fraction parameter of nanoparticles. It is observed that an insertion of nanoparticles leads to enhancement of heat transfer and attenuation of convective flow inside the cavity.

Keywords: natural convection; entropy generation; nanofluid; corner cooling; hot centered obstacle

1. Introduction

Solid blocks or bars can be used to control heat transfer as passive element in different shaped enclosures filled with nanofluids or pure fluids. This application can be observed in building design, electronic equipment, heat exchangers and some solar energy systems.

Buoyancy driven convection in a cavity filled with nanofluids with several pairs of heaters and coolers inside is analyzed computationally by Garoosi *et al.* [1]. They showed that the highest and the lowest impacts of design parameters, on the enhancement of heat transfer rate are caused by changing the position of heater and cooler and types of nanoparticles, respectively. Mahmoodi and Sebdani [2] solved the problem of free convection of Cu/water nanofluid in a cavity having adiabatic square bodies at its center with a numerical technique. They observed that for all Rayleigh numbers with the exception of Ra = 10^4, the average Nusselt number increases with increasing of nanoparticle volume fraction. Lee and Ha [3] considered a physical model with horizontal layer of fluid heated below and cold above with a conducting body placed at the center of the layer at different thermal conductivity ratio. They solved unsteady problem for different Rayleigh numbers. Multi-domain technique is used to handle a square-shaped conducting body. They presented the results for the case of dimensionless thermal conductivity of unity and also compared the results to those of pure natural convection. They also extended the similar geometry for different parameters [4]. Antar [5] calculated the heat transfer rate across building blocks in a cavity. He considered the conduction heat transfer in the block material

and both natural convection and radiation in the cavity and found that increasing the number of cavities while keeping the block width unchanged decreases the heat flux significantly. Martyushev and Sheremet [6] numerically analyzed natural convection combined with thermal surface radiation in an enclosure with a heat-conducting solid walls of finite thickness and having a local heat source. They revealed that regardless of the considered solid–fluid interface, the average convective Nusselt number increases with the Rayleigh number and thermal conductivity ratio, and decreases with the surface emissivity and ratio of solid wall thickness to cavity spacing. The average radiative Nusselt number increases with the Rayleigh number, surface emissivity and thermal conductivity ratio and decreases with ratio of solid wall thickness to cavity spacing. Arefmanesh *et al.* [7] used the meshless local Petrov–Galerkin method to make simulation the buoyancy-driven flow and heat transfer in a differentially-heated enclosure having a baffle attached to its higher temperature side wall. They found that the average Nusselt number descends with increasing the baffle amplitude and the cold wall average Nusselt number increases as the baffle number of undulation augments. Bakkas *et al.* [8] made a computer solution on the two-dimensional laminar steady natural convection in a horizontal channel with the upper wall maintained at a constant temperature and the lower one provided with rectangular heating blocks, periodically distributed. In their work, the blocks are connected with adiabatic segments and their surfaces are assumed to release a uniform heat flux. They demonstrated that, depending on the length of the computational domain and the governing parameters, different flow structures can be obtained. Tsay *et al.* [9] made a numerical analysis to obtain characteristics of heat transfer from a block heat source module at different angles in two-dimensional cabinets. They observed that the maximum reduction in hot spot temperature is about 41% when two air vents are constructed on the cabinet wall. The variation of module angle results in the maximum difference of the hot spot temperature is 17% for closed cabinet, and 10% for ventilated cabinet. Deng and Tang [10] simulated the heatline in a square solid inserted cavity. They used finite volume and heatline formulation to make visualization. Visualization results by streamlines and heatlines directly exhibit the nature of fluid flow and heat transfer in macroscopical level, and hence, provide a more vigorous means to discuss the convective heat transfer accordingly. Shuja *et al.* [11] used two porous blocks located in a square cavity to see the effects of these blocks on heat and fluid flow. The flow conditions at the cavity inlet are kept the same for all the cases simulated by authors and found that the Nusselt number enhances with the increasing porosity and heat flux. Kuznetsov and Sheremet [12] studied conjugate natural convection in a rectangular enclosure having heat-conducting solid walls with a heat-generating solid block inside the cavity located on the bottom wall in conditions of nonuniform heat exchange with an environment. The authors found that an increase in the Grashof number leads to formation of the steady thermal plume, and also is reflected in reduction of the cooling degree of the cavity. It is revealed that variation of the heat-generating sizes and position of the heat source allows to control the fluid flow and heat transfer inside the cavity. Braga and Lemos [13] compared the heat transfer characteristics across a square cavity partially filled with a fixed amount of conducting solid material. The solid phase is shaped into two different geometries, namely square and cylindrical rods, which are horizontally displaced inside the cavity. When comparing the two geometries for the same Rayleigh number, the study showed that the average Nusselt number for cylindrical rods are slightly lower than of square rods.

Effects of inclination angle on natural convection flow in a square enclosure with a centered internal conducting square block are analyzed by Das and Reddy [14] by using finite volume technique. Ray and Chatterjee [15] made a work on solid object inserted cavity with corner heating and found similar results.

Calculation of entropy generation is an excellent tool to obtain the energy losses inside the system. The basic theory of entropy generation is widely presented by Bejan [16–18]. The application of entropy generation is also reviewed by Oztop and Al-Salem [19]. A numerical study on natural convection and entropy generation in a porous enclosure with heat sources is presented by Lami and Praka [20]. Again, combination of entropy generation with nanofluid filled cavity block insertion is

given by Nayak *et al.* [21]. The entropy generation and Bejan number are evaluated to demonstrate the thermodynamic optimization of the mixed convection and they showed that the heat transfer rate increases remarkably by the addition of nanoparticles. Selimefendigil and Oztop [22] studied the natural convection and entropy generation of nanofluid filled cavity having different shaped obstacles with magnetic field effect. They observed that averaged heat transfer reduces by 21.35%, 32.85% and 34.64% for the cavity with circular, diamond and squared shaped obstacles, respectively, compared to cavity without obstacles at $Ra_I = 10^6$. It should be mentioned to this end the very good review paper on entropy generation in nanofluid flow by Mahian *et al.* [23].

The main aim of this study is to make a numerical analysis in a cavity filled with a nanofluid and a square heated object inserted. The cavity is cooled from the top wall and the left bottom corner. Thus, the study is a first attempt to control heat transfer via a passive element in a cavity with corner heater. Effects of entropy generation are studied to see the effective parameter on second law analysis of thermodynamics.

2. Basic Equations

Consider the free convection in a Cu-water nanofluid located in a square differentially heated cavity with hot centered block. A schematic geometry of the problem under investigation is shown in Figure 1, where $\overline{x}$ axis is measured in the horizontal direction along the bottom wall of the cavity and $\overline{y}$ axis is measured along the left vertical wall of the cavity and L is the size of the cavity. It is assumed that the top wall and left corner of the cavity are cooled with constant temperature T_c, while the centered square block is heated with constant temperature T_h. It is also assumed that other walls of the cavity are adiabatic. The walls of the cavity are assumed to be impermeable.

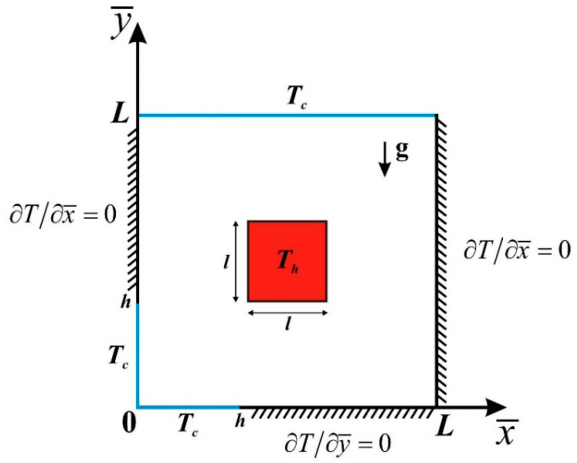

Figure 1. Physical model and coordinate system.

Except for the density, the properties of the fluid are taken to be constant. It is further assumed that the effect of buoyancy is included through the Boussinesq approximation. Under the above assumptions, the conservation equations for mass, momentum and thermal energy can be written as follows

$$\nabla \cdot \mathbf{V} = 0 \tag{1}$$

$$\rho_{\mathrm{nf}} (\mathbf{V}, \nabla) \mathbf{V} = -\nabla p + \mu_{\mathrm{nf}} \nabla^2 \mathbf{V} - (\rho\beta)_{\mathrm{nf}} (T - T_c) \mathbf{g} \tag{2}$$

$$(\rho C_p)_{\mathrm{nf}} (\mathbf{V}, \nabla T) = k_{\mathrm{nf}} \left(\frac{\partial^2 T}{\partial \overline{x}^2} + \frac{\partial^2 T}{\partial \overline{y}^2} \right) \tag{3}$$

The used physical properties of the nanofluid are described in detail earlier [24].

Equations (1)–(3) can be written in Cartesian coordinates as

$$\frac{\partial \overline{u}}{\partial \overline{x}} + \frac{\partial \overline{v}}{\partial \overline{y}} = 0 \tag{4}$$

$$\rho_{\mathrm{nf}} \left(\overline{u} \frac{\partial \overline{u}}{\partial \overline{x}} + \overline{v} \frac{\partial \overline{u}}{\partial \overline{y}} \right) = -\frac{\partial \overline{p}}{\partial \overline{x}} + \mu_{\mathrm{nf}} \left(\frac{\partial^2 \overline{u}}{\partial \overline{x}^2} + \frac{\partial^2 \overline{u}}{\partial \overline{y}^2} \right) \tag{5}$$

$$\rho_{\mathrm{nf}} \left(\overline{u} \frac{\partial \overline{v}}{\partial \overline{x}} + \overline{v} \frac{\partial \overline{v}}{\partial \overline{y}} \right) = -\frac{\partial \overline{p}}{\partial \overline{y}} + \mu_{\mathrm{nf}} \left(\frac{\partial^2 \overline{v}}{\partial \overline{x}^2} + \frac{\partial^2 \overline{v}}{\partial \overline{y}^2} \right) + (\rho\beta)_{\mathrm{nf}} g \left(T - T_c \right) \tag{6}$$

$$\frac{\partial T}{\partial t} + \overline{u} \frac{\partial T}{\partial \overline{x}} + \overline{v} \frac{\partial T}{\partial \overline{y}} = \alpha_{\mathrm{nf}} \left(\frac{\partial^2 T}{\partial \overline{x}^2} + \frac{\partial^2 T}{\partial \overline{y}^2} \right) \tag{7}$$

The existence of irreversibility source in the flow field such as the viscous dissipation effect and heat transfer causes the entropy generation. In Cartesian coordinates, the dimensional local entropy generation $\overline{S}_{gen}$ determined by Woods can be expressed as follows in the present study:

$$\overline{S}_{gen} = \frac{k_{\mathrm{nf}}}{T_0^2} \left[\left(\frac{\partial T}{\partial \overline{x}} \right)^2 + \left(\frac{\partial T}{\partial \overline{y}} \right)^2 \right] + \frac{\mu_{\mathrm{nf}}}{T_0} \left[2 \left(\frac{\partial u}{\partial \overline{x}} \right)^2 + 2 \left(\frac{\partial v}{\partial \overline{y}} \right)^2 + \left(\frac{\partial u}{\partial \overline{y}} + \frac{\partial v}{\partial \overline{x}} \right)^2 \right] \tag{8}$$

where $T_0 = 0.5 \left(T_c + T_h \right)$.

Equation (8) constitutes two terms: the first is the local entropy generation due to the heat transfer $\left(\overline{S}_{gen,ht} \right)$; and the second is the dimensional local entropy generation due to fluid friction $\left(\overline{S}_{gen,ff} \right)$.

Further, we introduce the following dimensionless variables

$$\begin{gathered} x = \overline{x}/L, \quad y = \overline{y}/L, \quad u = \overline{u}/\sqrt{g\beta \left(T_h - T_c \right) L}, \quad v = \overline{v}/\sqrt{g\beta \left(T_h - T_c \right) L}, \\ p = \overline{p}/\rho_{nf} g\beta \left(T_h - T_c \right) L, \quad \theta = \left(T - T_c \right) / \left(T_h - T_c \right) \end{gathered} \tag{9}$$

We are then left with the following equations

$$\frac{\partial u}{\partial x} + \frac{\partial v}{\partial y} = 0 \tag{10}$$

$$u \frac{\partial u}{\partial x} + v \frac{\partial u}{\partial y} = -\frac{\partial p}{\partial x} + H_1 (\varphi) \sqrt{\frac{\mathrm{Pr}}{Ra}} \left(\frac{\partial^2 u}{\partial x^2} + \frac{\partial^2 u}{\partial y^2} \right) \tag{11}$$

$$u \frac{\partial v}{\partial x} + v \frac{\partial v}{\partial y} = -\frac{\partial p}{\partial y} + H_1 (\varphi) \sqrt{\frac{\mathrm{Pr}}{Ra}} \left(\frac{\partial^2 v}{\partial x^2} + \frac{\partial^2 v}{\partial y^2} \right) + H_2 (\varphi) \theta \tag{12}$$

$$u \frac{\partial \theta}{\partial x} + v \frac{\partial \theta}{\partial y} = \frac{H_3 (\varphi)}{\sqrt{Ra \cdot \mathrm{Pr}}} \left(\frac{\partial^2 \theta}{\partial x^2} + \frac{\partial^2 \theta}{\partial y^2} \right) \tag{13}$$

The corresponding boundary conditions for these equations are given by

$$\begin{array}{lll} u = v = 0 & \text{on} & \text{solid walls} \\ \theta = 0 & \text{on} & \text{cooled walls} \\ \theta = 1 & \text{on} & \text{heated walls of centered body} \\ \partial\theta/\partial \mathbf{n} = 0 & \text{on} & \text{adiabatic walls} \end{array} \tag{14}$$

Here $\mathrm{Pr} = \mu_{\mathrm{f}} \left(\rho C_p \right)_{\mathrm{f}} / \left(\rho_{\mathrm{f}} k_{\mathrm{f}} \right)$ is the Prandtl number, $Ra = g \left(\rho\beta \right)_{\mathrm{f}} \left(T_h - T_c \right) L^3 / \left(\alpha_{\mathrm{f}} \mu_{\mathrm{f}} \right)$ is the Rayleigh number, and the functions $H_1 (\varphi)$, $H_2 (\varphi)$ and $H_3 (\varphi)$ are given by

$$H_1 (\varphi) = \frac{1}{(1-\varphi)^{2.5} \left[1 - \varphi + \varphi \rho_{\mathrm{p}} / \rho_{\mathrm{f}} \right]} \tag{15}$$

$$H_2(\varphi) = \frac{1-\varphi+\varphi(\rho\beta)_{\mathrm{p}}/(\rho\beta)_{\mathrm{f}}}{1-\varphi+\varphi\rho_{\mathrm{p}}/\rho_{\mathrm{f}}} \tag{16}$$

$$H_3(\varphi) = \frac{k_{\mathrm{p}}+2k_{\mathrm{f}}-2\varphi\left(k_{\mathrm{f}}-k_{\mathrm{p}}\right)}{\left[k_{\mathrm{p}}+2k_{\mathrm{f}}+\varphi\left(k_{\mathrm{f}}-k_{\mathrm{p}}\right)\right]\left[1-\varphi+\varphi(\rho S_p)_{\mathrm{p}}/(\rho S_p)_{\mathrm{f}}\right]} \tag{17}$$

These functions depend on the nanoparticles concentration ϕ and physical properties of the fluid and solid nanoparticles.

The dimensionless local entropy generation S_{gen} is obtained by using dimensionless parameters presented in Equation (9) given as:

$$\begin{aligned} S_{gen} &= \overline{S}_{gen}\frac{T_0^2L^2}{k_{\mathrm{f}}(T_h-T_c)^2} = \frac{k_{\mathrm{nf}}}{k_{\mathrm{f}}}\left[\left(\frac{\partial\theta}{\partial x}\right)^2+\left(\frac{\partial\theta}{\partial y}\right)^2\right]+ \\ &+\chi\left[2\left(\frac{\partial u}{\partial x}\right)^2+2\left(\frac{\partial v}{\partial y}\right)^2+\left(\frac{\partial u}{\partial y}+\frac{\partial v}{\partial x}\right)^2\right] = S_{gen,ht}+S_{gen,ff} \end{aligned} \tag{18}$$

In Equation (18), χ is the irreversibility factor. It is expressed as:

$$\chi = \frac{\mu_{\mathrm{nf}}T_0}{k_{\mathrm{f}}}\frac{g\beta L}{(T_h-T_c)} \tag{19}$$

The integration of Equation (18) in the entire computational domain gives the dimensionless average entropy generation, $S_{gen,avg}$, expressed as follows:

$$S_{gen,avg} = \frac{1}{\vartheta}\int S_{gen}d\vartheta = S_{gen,ht,avg}+S_{gen,ff,avg} \tag{20}$$

Further, the Bejan number *Be* is a parameter that shows the importance of heat transfer irreversibility in the domain and is defined as

$$Be = \frac{S_{gen,ht}}{S_{gen,ht}+S_{gen,ff}} \tag{21}$$

The relative global dominance of heat transfer irreversibility is predicted by Be_{avg} (average Bejan number) which can be defined as

$$Be_{avg} = \frac{S_{gen,ht,avg}}{S_{gen,avg}} \tag{22}$$

It may be noted that $Be_{avg} > 0.5$ shows that irreversibility due to heat transfer dominates in the flow. Fluid friction irreversibility dominates when $Be_{avg} < 0.5$ and when $Be_{avg} = 0.5$, the heat transfer and fluid friction entropy generation are equal.

The physical quantities of interest are the local Nusselt number $\left(Nu = -\frac{k_{\mathrm{nf}}}{k_{\mathrm{f}}}\frac{\partial\theta}{\partial\mathbf{n}}\right)$ along the heat source surface and the average Nusselt number, which is defined as

$$\overline{Nu} = -\frac{k_{\mathrm{nf}}L}{4k_{\mathrm{f}}l}\left(\int_{\frac{1-l/L}{2}}^{\frac{1+l/L}{2}}\left.\frac{\partial\theta}{\partial y}\right|_{y=\frac{1-l/L}{2}}dx+\int_{\frac{1-l/L}{2}}^{\frac{1+l/L}{2}}\left.\frac{\partial\theta}{\partial x}\right|_{x=\frac{1+l/L}{2}}dy+\int_{\frac{1-l/L}{2}}^{\frac{1+l/L}{2}}\left.\frac{\partial\theta}{\partial y}\right|_{y=\frac{1+l/L}{2}}dx+\int_{\frac{1-l/L}{2}}^{\frac{1+l/L}{2}}\left.\frac{\partial\theta}{\partial x}\right|_{x=\frac{1-l/L}{2}}dy\right) \tag{23}$$

3. Numerical Method and Validation

The governing Equations (10)–(13) with corresponding boundary conditions Equation (14) have been solved on the basis of finite volume method [25,26]. The convective terms are discretized applying the power scheme and the diffusive terms are discretized with the central scheme. The SIMPLE

algorithm is used to resolve the pressure–velocity coupling. The resulting algebraic equations systems for momentum equations were solved applying the line by line method with the implicit scheme of altering directions. The resulting algebraic equations system for energy equation was solved applying the explicit Buleev method for three-dimensional seven-point equations [27]. If values of mass balance for each control volume as well as the residual values of the different equations are sufficiently low overall convergence is obtained (typically 10^{-6}). The above convergence criterion assures an acceptable solution [28,29]. The computer code was developed by authors using the C++ programming language.

The performance of part concerning natural convection inside the square cavity with a heated centered body was tested against the results of Asan [28]. Figures 2 and 3 show a good agreement between the obtained streamlines and isotherms for different values of the Rayleigh number and solid block size and the numerical data of Asan [28]. The average Nusselt numbers of internal hot square block, which are also obtained by the present code, are compared with results of Asan [28] in Table 1.

Table 1. Comparison of present calculations with those of Asan [28].

Authors	$Ra = 10^3$	$Ra = 10^4$	$Ra = 10^5$	$Ra = 10^6$
Asan [28]	5.813	5.995	6.188	10.425
Present results	5.913	5.924	6.006	10.598

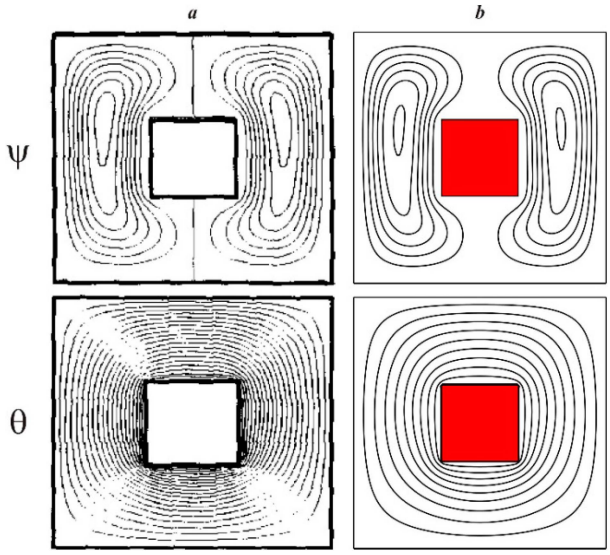

Figure 2. Comparison of streamlines ψ and isotherms θ for $Ra = 10^4$, $l/L = 0.3$: numerical data of Asan [28] (***a***) and the present results (***b***).

The performance of entropy generation part of the model was tested against the results of Ilis *et al.* [29] and Bhardwaj *et al.* [30] for steady-state natural convection in a differentially heated square cavity filled with the regular fluid for Prandtl number 0.7. Figures 4 and 5 show a good agreement between the obtained fields of local entropy generation due to heat transfer and fluid friction with $\chi = 10^{-4}$ for different Rayleigh numbers and the numerical data of Ilis *et al.* [29] and Bhardwaj *et al.* [30].

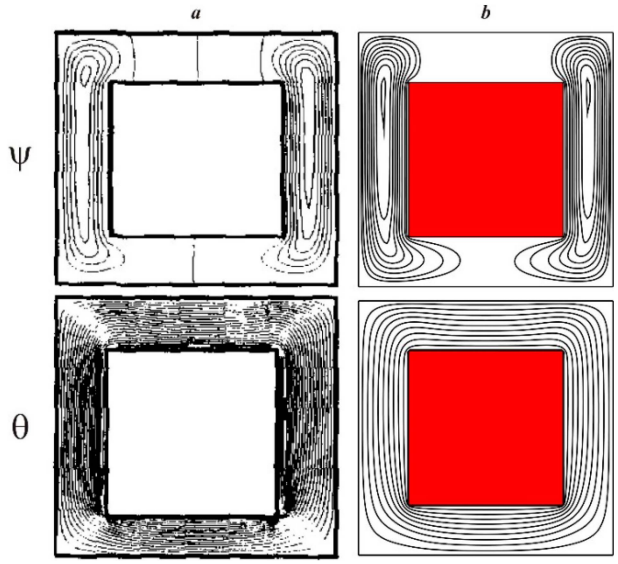

Figure 3. Comparison of streamlines ψ and isotherms θ for $Ra = 10^5$, $l/L = 0.6$: numerical data of Asan [28] (***a***) and the present results (***b***).

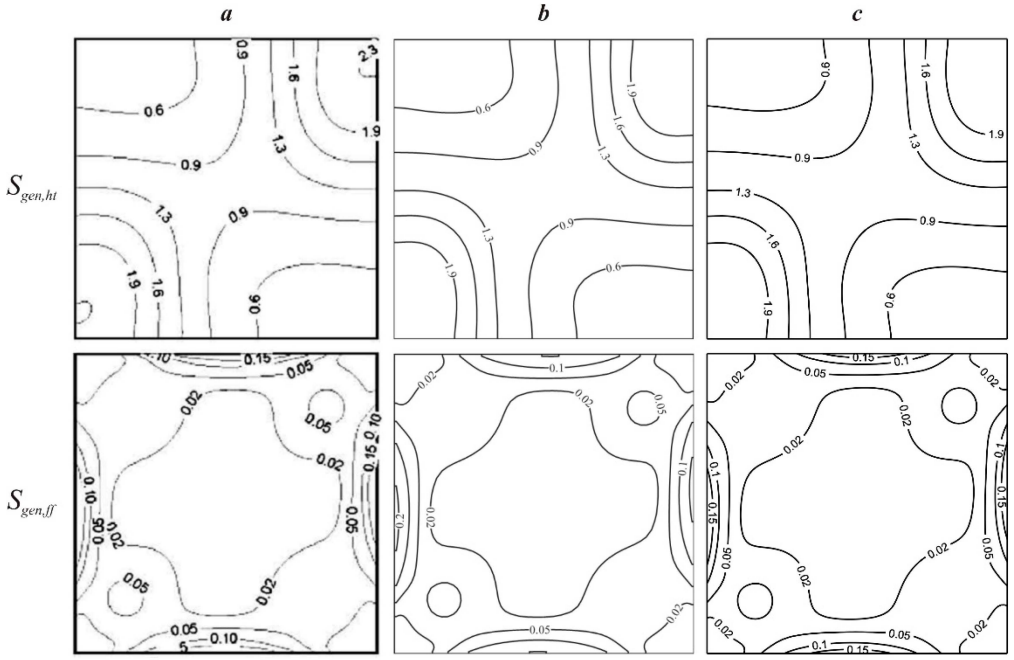

Figure 4. Comparison of local entropy generation due to heat transfer $S_{gen,ht}$ and fluid friction $S_{gen,ff}$ for $Ra = 10^3$: numerical data of Ilis *et al.* [29] (***a***); numerical data of Bhardwaj *et al.* [30] (***b***); and the present results (***c***).

For the purpose of obtaining grid independent solution, a grid sensitivity analysis is performed. The grid independent solution was performed by preparing the solution for steady free convection in a square cavity with centered heated filled with a Cu-water nanofluid at $Ra = 10^5$, $Pr = 6.82$, $\phi = 0.02$, $l/L = 0.3$, $h/L = 0.5$. Three cases of the uniform grid are tested: a grid of 80 × 80 points, a grid of 100 × 100 points, a grid of 120 × 120 points, and a grid of 140 × 140 points. Figure 6 shows an effect of the mesh parameters on the temperature profiles at middle cross-section $x = 0.5$.

On the basis of the conducted verifications, the uniform grid of 120 × 120 points has been selected for the following analysis.

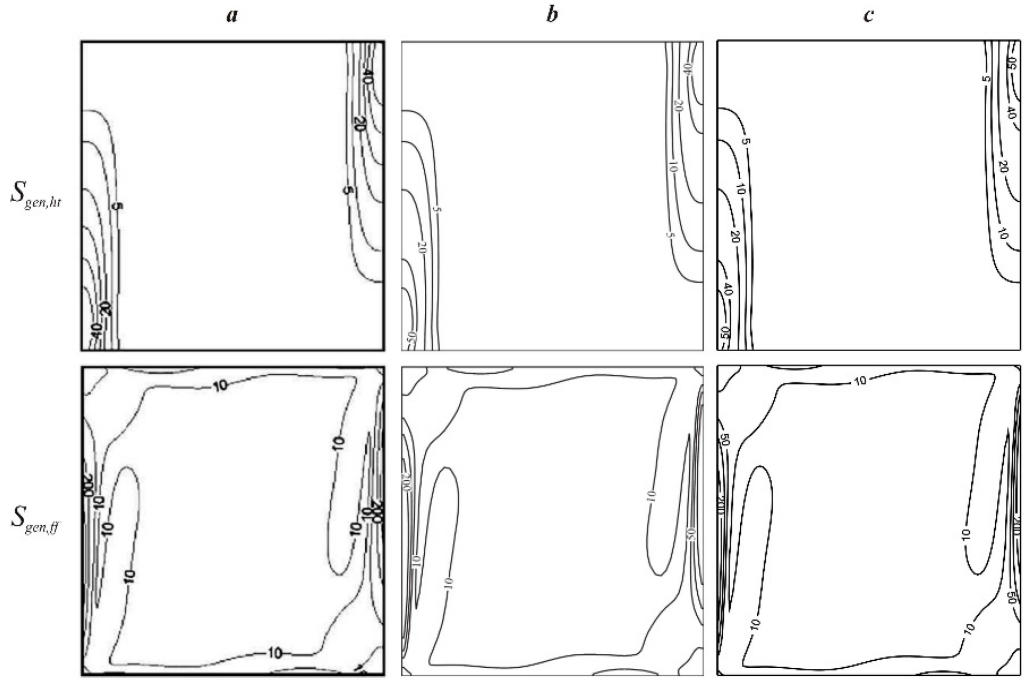

Figure 5. Comparison of local entropy generation due to heat transfer $S_{gen,ht}$ and fluid friction $S_{gen,ff}$ for $Ra = 10^5$: numerical data of Ilis *et al.* [29] (***a***); numerical data of Bhardwaj *et al.* [30] (***b***); and the present results (***c***).

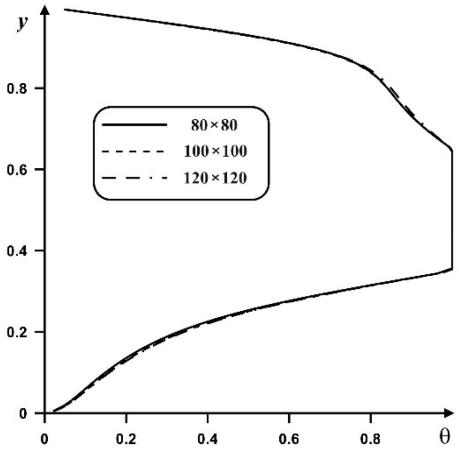

Figure 6. Variation of the temperature profiles at $x = 0.5$ *versus* the mesh parameters.

4. Results and Discussion

Numerical analysis has been conducted at the following values of the governing parameters: Rayleigh number ($Ra = 10^3$–10^6), solid volume fraction parameter of nanoparticles ($\varphi = 0.0$–0.05), dimensionless centered solid block size ($l/L = 0.2 - 0.6$) and dimensionless cooler length in x and y directions ($h/L = 0.25 - 0.75$). Particular efforts have been focused on the effects of these governing parameters on the fluid flow and heat transfer inside the cavity. Streamlines, isotherms, entropy generation profiles, average Nusselt numbers, average total entropy generation and average Bejan number for different values of key parameters mentioned above are illustrated in Figures 7–12.

Figure 7 presents distributions of streamlines, isotherms, local entropy generation due to heat transfer and fluid friction inside the cavity for different values of the Rayleigh number at $l/L = 0.2$, $h/L = 0.25$, $\phi = 0.03$. Regardless of the Rayleigh number values, two convective

cells are formed inside the cavity astride a heat source. It should be noted that one can find ascending flows close to the centered heater and descending flows near the vertical adiabatic wall. These two vortices characterize the presence of major motion from the left side of the heat source and minor circulation from the right side of the heater. An appearance of such division is due to the presence of the cooler in the left bottom corner that intensifies the left convective circulation: $|\psi|_{\max}^{Ra=10^3} = 0.00173 < |\psi|_{\max}^{Ra=10^4} = 0.0042 < |\psi|_{\max}^{Ra=10^5} = 0.0116$. An increase in Ra leads to an intensification of convective flow with a displacement of the convective cores along the vertical direction. One can find that for $Ra = 10^4$ there are two convective cores inside the left vortex that can be explained by the effect of the cooling from both the top wall and the left bottom corner. At the same time, an increase in Ra leads to an intensification of the right convective cell with some deformation of this vortex in the bottom part from the main circulation.

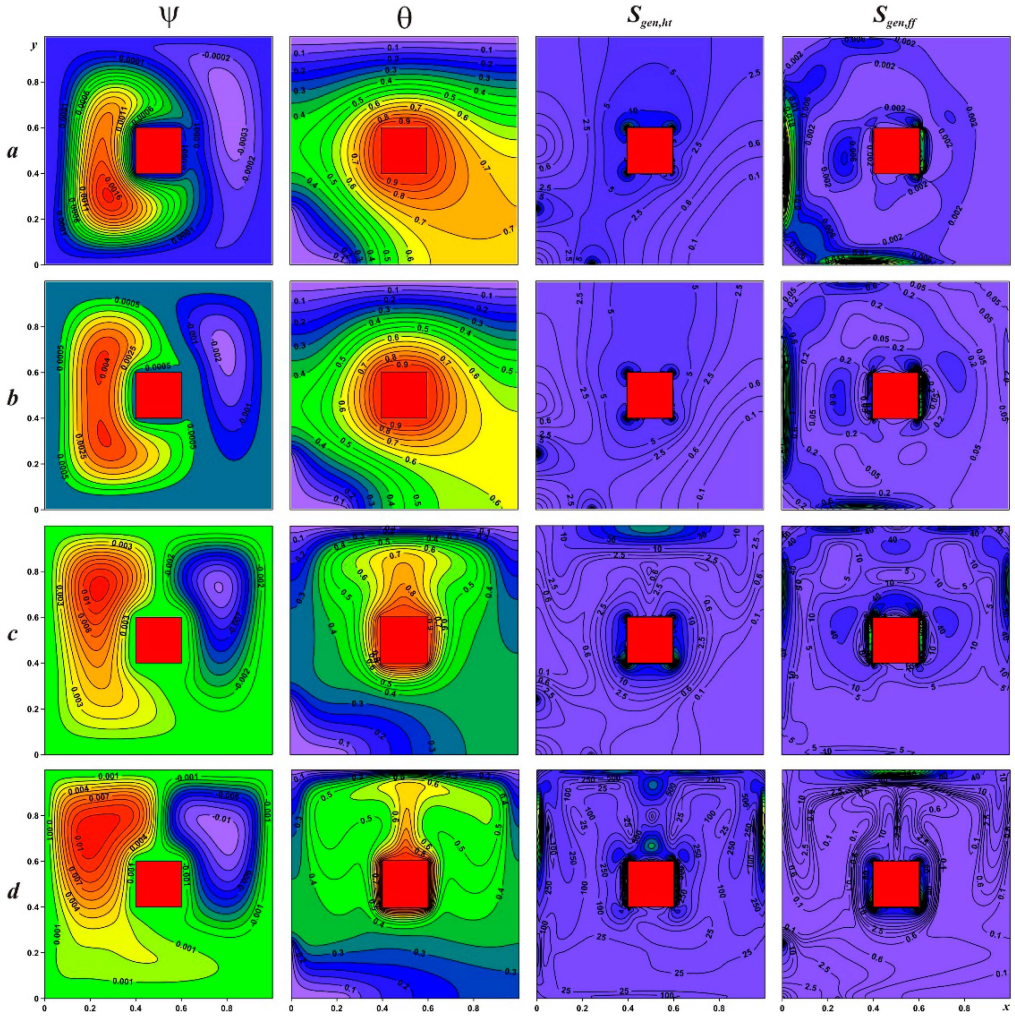

Figure 7. Streamlines ψ, isotherms θ, local entropy generation due to heat transfer $S_{gen,ht}$, local entropy generation due to fluid friction $S_{gen,ff}$ for $l/L = 0.2$, $h/L = 0.25$, $\phi = 0.03$: $Ra = 10^3$ (***a***); $Ra = 10^4$ (***b***); $Ra = 10^5$ (***c***); and $Ra = 10^6$ (***d***).

The temperature fields are also changed with Ra. For small values of the Rayleigh number ($Ra = 10^3$ and 10^4, Figure 7a,b), the main heat transfer regime is a heat conduction. This regime is characterized by isotherms that are parallel to the top horizontal isothermal wall. At the same time, one can find that heat fluxes from the top and corner coolers at $Ra = 10^3$ deform the heat flux from the centered heater. Therefore the main heating occurs in the right corner where the walls are adiabatic.

An increase in Ra (= 10^4) leads to less intensive heating of the right corner of the cavity due to an appearance of convective heat flux and distributions of isotherms also along the vertical axis. The latter illustrates weak counteraction to the penetration of cold temperature from the top wall inside the cavity. In the case of $Ra = 10^5$ (Figure 7c) a thermal plume over the heat source is formed characterizing an amplification of the buoyancy force. Such development of the heat flux over the heat source prevents to the cooling of the cavity from the top wall, while cooling from the corner occurs in the bottom part of the cavity along the horizontal axis. It is worth noting that, for this value of the Rayleigh number, the thermal plume is a symmetric distribution of isotherms over the heat source. Further increase in Ra leads to an intensification of heat removal from the central heater along the vertical axis with asymmetric distributions of isotherms in this plume. At the same time, one can find more essential cooling of the bottom part of the cavity at $Ra = 10^6$ (Figure 7d).

For the analyzed problem, it is interesting to define the entropy generation areas inside the cavity. Figure 7 shows also the local entropy generation due to heat transfer $S_{gen,ht}$ and fluid friction $S_{gen,ff}$. For the small values of the Rayleigh number ($Ra = 10^3$ and 10^4) distributions of $S_{gen,ht}$ and $S_{gen,ff}$ are uniform in general with the exception of the heater and cooler end points. For this Rayleigh number value the intensive entropy generation places due to heat transfer are the end points of the heater and corner cooler. Such distributions can be explained by the presence of some singularities in these points such as salient points for the heater or border points between isothermal and adiabatic conditions. At the same time, more intensive entropy generation due to fluid friction occurs close to the cooler and vertical walls of the heater that can be explained by the presence of essential velocity gradients in these parts of the cavity. An increase in the Rayleigh number leads to an intensification of the entropy generation inside the cavity. Formation of the thermal plume over the heater and a thin thermal boundary layer around the heater leads to an intensification of the entropy generation due to fluid friction in these zones. Moreover it is possible to conclude that for high values of the Rayleigh number distributions of local entropy generation are the similar to the distributions of isotherms inside the thermal plume.

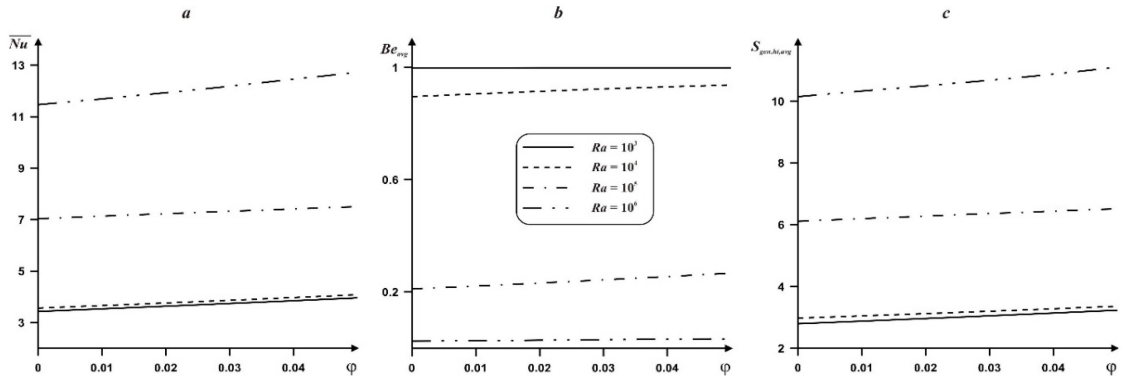

Figure 8. Variation of the average Nusselt number (***a***); the average Bejan number (***b***); and the average entropy generation due to heat transfer (***c***) *versus* the nanoparticle volume fraction and Rayleigh number for $l/L = 0.2$, $h/L = 0.25$.

An intensification of the convective heat transfer rate around the heater Equation (22) with buoyancy force is presented in Figure 8. It should be noted that the average Bejan number reflects the ratio between the average entropy generation due to heat transfer and average total entropy generation. For low values of Ra when convective flow is characterized by small velocities and the entropy generation occurs due to heat transfer, therefore we have $Be_{avg} \approx 1$. An increase in Ra greater than 10^5 leads to an essential decrease in the average Bejan number (Figure 9b) with significant increase in the average total entropy generation (Figure 9c). Such behavior is due to an intensification of convective flow with an increase in the Rayleigh dissipative function. It should be noted that an increase in $\overline{Nu}$ with Ra is similar qualitatively to an increase in $S_{gen,avg}$ with the Rayleigh number.

An influence of the nanoparticles volume fraction on the isolines of stream function, temperature, local entropy generation due to heat transfer and fluid friction is presented in Figure 9 for $Ra = 10^5$, $l/L = 0.2$, $h/L = 0.25$. An increase in ϕ leads to inessential changes in the local entropy generation while streamlines and isotherms have some changes. It should be noted that an increase in the concentration of nanoparticles leads to an attenuation of the convective flow taking into account the values of $|\psi|_{\max}$: $|\psi|_{\max}^{\varphi=0} = 0.0118 > |\psi|_{\max}^{\varphi=0.05} = 0.0113$. At the same time, one can find less intensive cooling of the bottom part with ϕ taking into account the position of isotherm θ = 0.3.

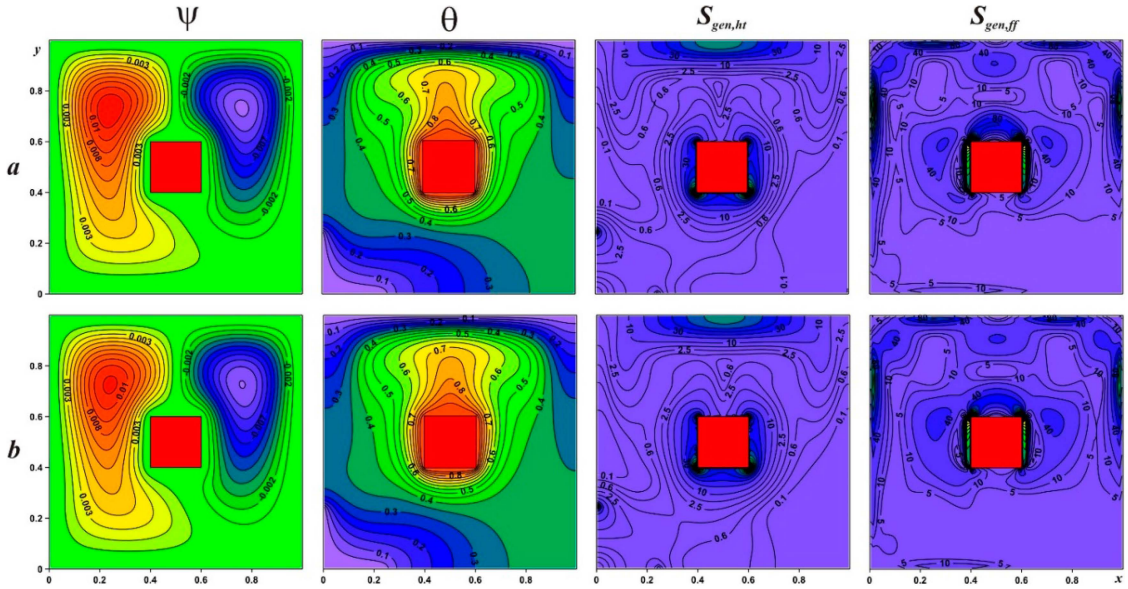

Figure 9. Streamlines ψ, isotherms θ, local entropy generation due to heat transfer $S_{gen,ht}$, local entropy generation due to fluid friction $S_{gen,ff}$ for $Ra = 10^5$, $l/L = 0.2$, $h/L = 0.25$: ϕ = 0.0 (***a***) and ϕ = 0.05 (***b***).

The effect of the concentration of nanoparticles on the average Nusselt and Bejan numbers and total entropy generation is presented in Figure 8. It is worth noting that an increase in ϕ leads to an increase in all these parameters. More intensive increase in $\overline{Nu}$ and $S_{gen,avg}$ with nanoparticles volume fraction occurs for high values of Ra. As has been mentioned above, for high values of Ra, $Be_{avg} \ll 0.5$, therefore fluid friction irreversibility dominates.

The effect of the dimensionless centered solid block size on the distributions of local parameters is demonstrated in Figure 10. An increase in l/L leads to essential changes in all parameters. It is worth noting that an increase in l/L leads to a decrease in the distance between the top cold wall and the hot surface of the centered block therefore we have a local Rayleigh–Benard problem for narrow channel. As a result such narrowing leads to a formation of several convective cells of low intensity in this nanofluid gap [28]. Moreover, all these recirculations illustrate an appearance of ascending and descending thermal plumes over the heat source while under the heat source one can find heat conduction as a dominating heat transfer regime.

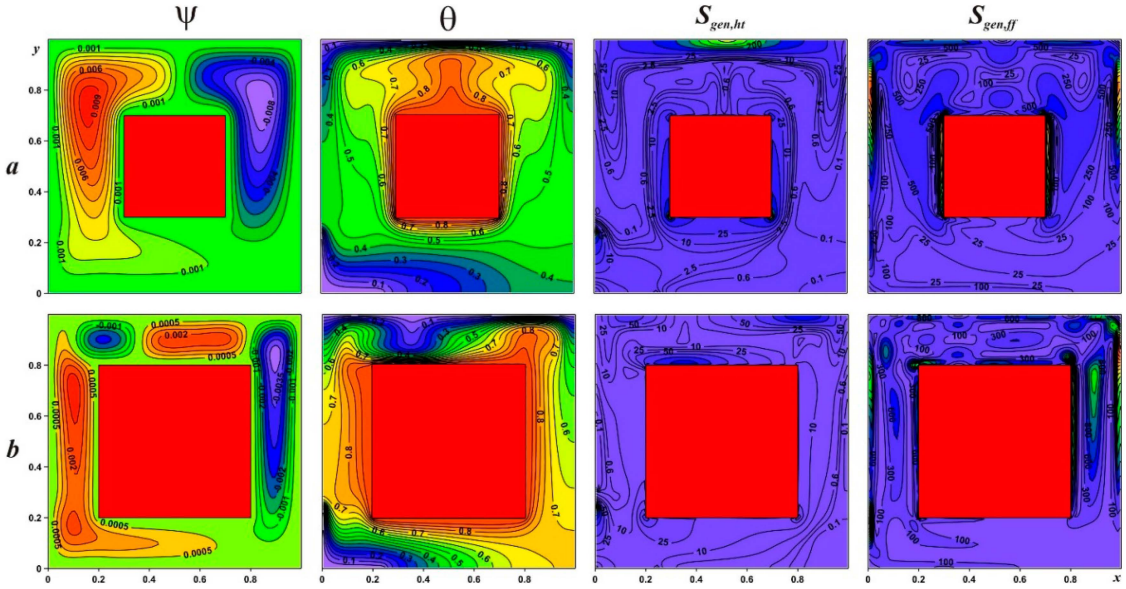

Figure 10. Streamlines ψ, isotherms θ, local entropy generation due to heat transfer $S_{gen,ht}$, local entropy generation due to fluid friction $S_{gen,ff}$ for $Ra = 10^6$, $h/L = 0.25$, $\phi = 0.03$: $l/L = 0.4$ (***a***) and $l/L = 0.6$ (***b***).

An increase in the dimensionless centered solid block size leads to an essential decrease in the average Nusselt number (Figure 11a) and an increase in the average Bejan number (Figure 11b) and average total entropy generation (Figure 11c). A reduction of $\overline{Nu}$ can be explained by an attenuation of the convective flow and also by narrowing of the nanofluid cavity. An increase in Be_{avg} and $S_{gen,avg}$ with l/L is due to an increase in the average entropy generation due to heat transfer inside the cavity where one can find an interaction of boundary layers in the case of narrow nanofluid zones.

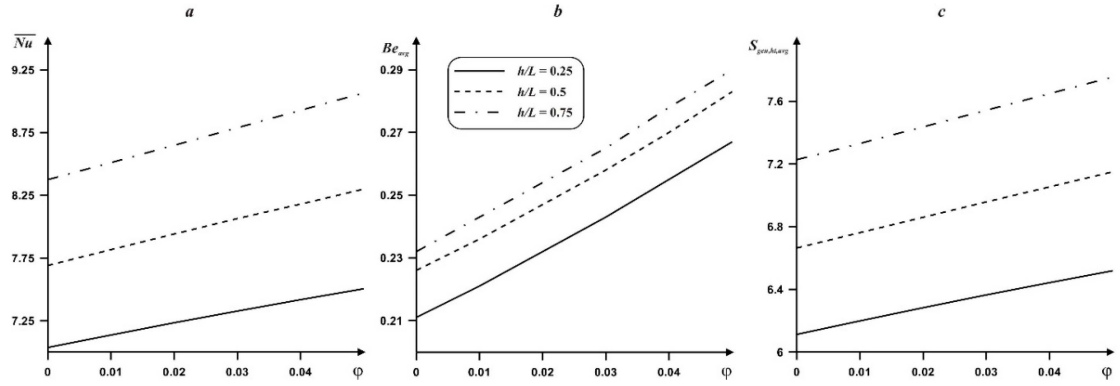

Figure 11. Variation of the average Nusselt number (***a***); the average Bejan number (***b***); and the average entropy generation due to heat transfer (***c***) *versus* the nanoparticle volume fraction and dimensionless centered solid block size for $Ra = 10^6$, $h/L = 0.25$.

Figure 12 illustrates an influence of the dimensionless cooler length in x and y directions on the heat transfer rate, average Bejan number and average total entropy generation. An increase in h/L leads to an enhancement of the heat transfer rate, average Bejan number and average total entropy generation due to an increase in the temperature gradient and as a result an increase in the convective velocity. The latter leads to an increase in the entropy generation due to heat transfer.

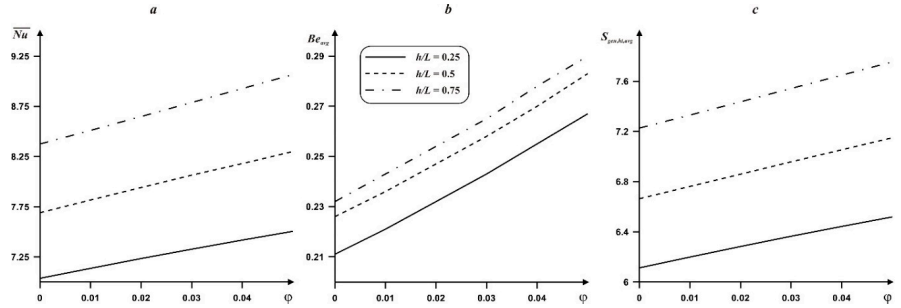

Figure 12. Variation of the average Nusselt number (***a***); the average Bejan number (***b***); and the average entropy generation due to heat transfer (***c***) *versus* the nanoparticle volume fraction and dimensionless cooler length for $Ra = 10^5$, $l/L = 0.2$.

5. Conclusions

The steady problem of entropy generation and natural convection of Cu/water nanofluid within a differentially heated cavity with a centered hot square block and corner cooler was formulated in dimensionless primitive variables using the nanofluid model proposed by Tiwari and Das and solved numerically on the basis of finite volume method of a second-order accuracy. Profiles of stream function, temperature, local entropy generation due to heat transfer and local entropy generation due to fluid friction in a wide range of governing parameters have been obtained. The main findings can be listed as:

(1) An increase in the Rayleigh number leads to an intensification of convective flow and heat transfer, and a reduction of the average Bejan number due to an enhancement of fluid friction. An increase in $\overline{Nu}$ with Ra is similar qualitatively to an increase in $S_{gen,avg}$ with the Rayleigh number.

(2) An increase in the nanoparticles volume fraction leads to an attenuation of convective flow and less intensive cooling of the bottom part of the cavity. Average Nusselt and Bejan numbers and average total entropy generation are increasing functions of ϕ.

(3) An increase in the dimensionless centered solid block size leads to a formation of several convective cells of low intensity in nanofluid gap between top cold wall and top surface of the heater. In addition, the heat transfer rate decreases with l/L while average Bejan number and average total entropy generation are an increasing functions of l/L.

(4) All considered average parameters are increasing functions of the dimensionless cooler length due to a widening of the heat sink surface.

Acknowledgments: This work of Mikhail A. Sheremet was conducted as a government task of the Ministry of Education and Science of the Russian Federation, Project Number 13.1919.2014/K. The authors wish to express their very sincere thanks to the very competent Reviewers for the very good comments and suggestions.

Author Contributions: Mikhail A. Sheremet conducted the simulations for the paper and wrote some sections of the manuscript. Hakan F. Oztop, Ioan Pop and Nidal Abu-Hamdeh prepared the Introduction part, wrote some other sections and analyzed the obtained numerical data. All authors contributed to the conclusions and assisted with reviewing and revising the manuscript.

Conflicts of Interest: The authors declare no conflict of interest.

Abbreviations

Be	local Bejan number
Be_{avg}	average Bejan number
C_p	specific heat at constant pressure
$\mathbf{g}$	gravitational acceleration vector
$H_1(\varphi)$, $H_2(\varphi)$, $H_3(\varphi)$	special functions
k	thermal conductivity

L	size of the cavity
Nu	local Nusselt number
$\overline{Nu}$	average Nusselt number
p	dimensionless pressure
$\overline{p}$	dimensional pressure
Pr	Prandtl number
Ra	Rayleigh number
$\overline{S_{gen}}$	dimensional local entropy generation
S_{gen}	dimensionless local entropy generation
$S_{gen,avg}$	dimensionless average entropy generation
$S_{gen,ff}$	dimensionless local entropy generation due to fluid friction
$S_{gen,ff,avg}$	dimensionless average entropy generation due to fluid friction
$S_{gen,ht}$	dimensionless local entropy generation due to the heat transfer
$S_{gen,ht,avg}$	dimensionless average entropy generation due to heat transfer
T	dimensional nanofluid temperature
T_c	temperature of the cold walls
T_h	temperature of the heat source
$\mathbf{V}$	velocity vector
u, v	dimensionless velocity components
$\overline{u}, \overline{v}$	dimensional velocity components
x, y	dimensionless Cartesian coordinates
$\overline{x}, \overline{y}$	dimensional Cartesian coordinates
Greek symbols	
α	thermal diffusivity
β	thermal expansion coefficient
θ	dimensionless temperature
ϑ	volume occupied by the nanofluid
μ	dynamic viscosity
ρ	density
ρC_p	heat capacitance
$\rho\beta$	buoyancy coefficient
φ	uniform concentration of the nanoparticles
χ	irreversibility factor
ψ	dimensionless stream function
Subscript	
c	cold
f	fluid
nf	nanofluid

References

1. Garoosi, F.; Bagheri, G.; Talebi, F. Numerical simulation of natural convection of nanofluids in a square cavity with several pairs of heaters and coolers (HACs) inside. *Int. J. Heat Mass Transf.* **2013**, *67*, 362–376. [CrossRef]
2. Mahmoodi, M.; Sebdani, S.M. Natural convection in a square cavity containing a nanofluid and an adiabatic square block at the center. *Superlattices Microstruct.* **2012**, *52*, 261–275. [CrossRef]
3. Lee, J.R.; Ha, M.Y. A numerical study of natural convection in a horizontal enclosure with a conducting body. *Int. J. Heat Mass Transf.* **2005**, *48*, 3308–3318. [CrossRef]
4. Lee, J.R.; Ha, M.Y. Numerical simulation of natural convection in a horizontal enclosure with a heat-generating conducting body. *Int. J. Heat Mass Transf.* **2006**, *49*, 2684–2702. [CrossRef]
5. Antar, M.A. Thermal radiation role in conjugate heat transfer across a multiple-cavity building block. *Energy* **2010**, *35*, 3508–3516. [CrossRef]

6. Martyushev, S.G.; Sheremet, M.A. Conjugate natural convection combined with surface thermal radiation in an air filled cavity with internal heat source. *Int. J. Ther. Sci.* **2014**, *76*, 51–67. [CrossRef]
7. Arefmanesh, A.; Najafi, M.; Musavi, S.H. Buoyancy-driven fluid flow and heat transfer in a square cavity with a wavy baffle—Meshless numerical analysis. *Eng. Anal. Bound. Elem.* **2013**, *37*, 366–382. [CrossRef]
8. Bakkas, M.; Amahmid, A.; Hasnaoui, M. Numerical study of natural convection heat transfer in a horizontal channel provided with rectangular blocks releasing uniform heat flux and mounted on its lower wall. *Energy Convers. Manag.* **2008**, *49*, 2757–2766. [CrossRef]
9. Tsay, Y.L.; Cheng, J.C.; Zhuang, Y.L. Natural convective characteristics of a heat source module at different angles in the closed and ventilated cabinets. *Int. Commun. Heat Mass Transf.* **2010**, *37*, 1048–1056. [CrossRef]
10. Deng, Q.H.; Tang, G.F. Numerical visualization of mass and heat transport for conjugate natural convection/heat conduction by streamline and heatline. *Int. J. Heat Mass Transf.* **2002**, *45*, 2373–2385. [CrossRef]
11. Shuja, S.Z.; Yilbas, B.S.; Kassas, M. Flow over porous blocks in a square cavity: Influence of heat flux and porosity on heat transfer rates. *Int. J. Ther. Sci.* **2009**, *48*, 1564–1573. [CrossRef]
12. Kuznetsov, G.V.; Sheremet, M.A. Conjugate natural convection in an enclosure with a heat source of constant heat transfer rate. *Int. J. Heat Mass Transf.* **2011**, *54*, 260–268. [CrossRef]
13. Braga, E.J.; Lemos, M.J.S. Laminar natural convection in cavities filled with circular and square rods. *Int. Commun. Heat Mass Transf.* **2005**, *32*, 1289–1297. [CrossRef]
14. Das, M.K.; Reddy, K.S.K. Conjugate natural convection heat transfer in an inclined square cavity containing a conducting block. *Int. J. Heat Mass Transf.* **2006**, *49*, 4987–5000. [CrossRef]
15. Ray, S.; Chatterjee, D. MHD mixed convection in a lid-driven cavity including heat conducting solid object and corner heaters with Joule heating. *Numer. Heat Transf. A* **2014**, *66*, 530–550. [CrossRef]
16. Bejan, A. Second law analysis in heat transfer. *Energy Int. J.* **1980**, *5*, 721–732. [CrossRef]
17. Bejan, A. *Entropy Generation through Heat and Fluid Flow*; John Wiley & Sons, Inc.: Hoboken, NJ, USA, 1982.
18. Bejan, A. *Entropy Generation Minimization: The Method of Thermodynamic Optimization of Finite-Size Systems and Finite-Time Processes*; CRC Press: New York, NY, USA, 1995.
19. Oztop, H.F.; Al-Salem, K. A review on entropy generation in natural and mixed convection heat transfer for energy systems. *Renew. Sustain. Energy Rev.* **2012**, *16*, 911–920. [CrossRef]
20. Lami, P.A.K.; Praka, K.A. A numerical study on natural convection and entropy generation in a porous enclosure with heat sources. *Int. J. Heat Mass Transf.* **2014**, *69*, 390–407. [CrossRef]
21. Nayak, R.K.; Bhattacharyya, S.; Pop, I. Numerical study on mixed convection and entropy generation of Cu–water nanofluid in a differentially heated skewed enclosure. *Int. J. Heat Mass Transf.* **2015**, *85*, 620–634. [CrossRef]
22. Selimefendigil, F.; Öztop, H.F. Natural convection and entropy generation of nanofluid filled cavity having different shaped obstacles under the influence of magnetic field and internal heat generation. *J. Taiwan Inst. Chem. Eng.* **2015**, *56*, 42–56. [CrossRef]
23. Mahian, O.; Kianifar, A.; Kleinstreuer, C.; Al-Nimr, M.A.; Pop, I.; Sahin, A.Z.; Wongwises, S. A review on entropy generation in nanofluid flow. *Int. J. Heat Mass Transf.* **2013**, *65*, 514–532. [CrossRef]
24. Sheremet, M.A.; Grosan, T.; Pop, I. Free convection in a square cavity filled with a porous medium saturated by nanofluid using Tiwari and Das' nanofluid model. *Transp. Porous Media* **2015**, *106*, 595–610. [CrossRef]
25. Ferziger, J.H.; Peric, M. *Computational Methods for Fluid Dynamics*; Springer: Berlin, Germany, 2002.
26. Versteeg, H.K.; Malalasekera, W. *An Introduction to Computational Fluid Dynamics. The Finite Volume Method*; John Wiley & Sons, Inc.: Hoboken, NJ, USA, 1995.
27. Buleev, N.I. The method of incomplete factorization for solving two-dimensional and three-dimensional equations of the diffusion type. *USSR Comput. Math. Math. Phys.* **1970**, *10*, 307–310. [CrossRef]
28. Asan, H. Natural convection in an annulus between two isothermal concentric square ducts. *Int. Commun. Heat Mass Transf.* **2000**, *27*, 367–376. [CrossRef]
29. Ilis, G.G.; Mobedi, M.; Sunden, B. Effect of aspect ratio on entropy generation in a rectangular cavity with differentially heated vertical walls. *Int. Commun. Heat Mass Transf.* **2008**, *35*, 696–703. [CrossRef]
30. Bhardwaj, S.; Dalal, A.; Pati, S. Influence of wavy wall and non-uniform heating on natural convection heat transfer and entropy generation inside porous complex enclosure. *Energy* **2015**, *79*, 467–481. [CrossRef]